GEOPHYSICS, VOL. 60, NO. 4 (JULY-AUGUST 1995); P. 1203–1216, 11 FIGS., 2 TABLES.

Anisotropic wave propagation through finite-difference grids

Heiner Igel*, Peter Mora‡, and Bruno Riollet**

ABSTRACT

An algorithm is presented to solve the elastic-wave equation by replacing the partial differentials with finite differences. It enables wave propagation to be simulated in three dimensions through generally anisotropic and heterogeneous models. The space derivatives are calculated using discrete convolution sums, while the time derivatives are replaced by a truncated Taylor expansion. A centered finite difference scheme in cartesian coordinates is used for the space derivatives leading to staggered grids. The use of finite difference approximations to the partial derivatives results in a frequency-dependent error in the group and phase velocities of waves. For anisotropic media, the use of staggered grids implies that some of the elements of the stress and strain tensors must be interpolated to calculate the Hook sum. This interpolation induces an additional error in the wave properties. The overall error depends on the precision of the derivative and interpolation operators, the anisotropic symmetry system, its orientation and the degree of anisotropy. The dispersion relation for the homogeneous case was derived for the proposed scheme. Since we use a general description of convolution sums to describe the finite difference operators, the numerical wave properties can be calculated for any space operator and an arbitrary homogeneous elastic model. In particular, phase and group velocities of the three wave types can be determined in any direction. We demonstrate that waves can be modeled accurately even through models with strong anisotropy when the operators are properly designed.

INTRODUCTION

Until recently, finite difference schemes for reasonably sized 3-D earth models were inconceivable because of hardware limitations. Although 3-D elastic modeling has been implemented on serial hardware (Reshef et al., 1988), large scale 3-D modeling has become feasible only since the advent of massively parallel computers (Mora, 1989). Finite difference schemes naturally map onto the architecture of parallel hardware. This work is motivated by the need to find accurate *local* finite difference operators for the general anisotropic case that are efficient using the nearest neighbor communications of massively parallel computers. Finite difference operators can be expressed in a general way as convolution sums. The accuracy and design of such operators has been discussed in Holberg (1987) for models consisting of acoustic or isotropic elastic material. In principle, it is straightforward to introduce anisotropy into a finite difference scheme although an additional error may occur in some cases; e.g., when the grids are staggered, the elements of the stress and strain tensors are not all defined at the same location necessitating interpolations to compute the Hooke sum.

Note that these interpolations may be avoided in theory by specifying all components of displacement on one staggered grid and all components of stress and strain at another staggered grid. However, this option is undesirable because: (1) it requires ≈3.7 times more memory in 3-D thus severely restricting model sizes, and (2) the solutions propagating in different grids become independent when the medium is isotropic, and they are only weakly connected for weak anisotropy suggesting the additional grids are unnecessary and possibly even detrimental to the precision. In Figure 1 a grid cell shows where the fields are known at all grid points.

Manuscript received by the Editor October 28, 1992; revised manuscript received August 24, 1993.
*Formerly Département de Sismologie, Institut de Physique du Globe, 4 Place Jussieu, F-75252 Paris Cedex 05, France; presently Institute of Theoretical Geophysics, Dept. of Earth Sciences, University of Cambridge, Downing Street, Cambridge CB2 3EQ, United Kingdom.
‡Formerly Département de Sismologie, Institut de Physique du Globe, 4 Place Jussieu, F-75252 Paris Cedex 05, France; presently Dept. of Earth Sciences, University of Queensland, St. Lucia, Brisbane, Australia.
**Département de Sismologie, Institut de Physique du Globe, 4 Place Jussieu, F-75252 Paris Cedex 05, France.

The suggested staggering of the fields can be seen in Figure 2.

The main criteria for choosing a finite difference approach are high accuracy in modeling the physical properties one is interested in and being computationally feasible with respect to the available hardware. Pseudospectral methods are attractive since the space operators are exact up to the Nyquist frequency. However, they require Fourier transforms of the fields to be made, which are computationally expensive for large 3-D models. Moreover, taking the Fourier transform means that each point in the 3-D model interacts with every other point. In some sense, this is unphysical as interaction in dynamic elasticity is of a local nature. Thus it is not surprising that local operators, which take into account only interaction between the particles and their nearest neighbors, are accurate for long wavelengths.

These considerations suggest that finite-difference solutions to the wave equation are well suited for implementation on hardware architectures with massive parallelism since nearest neighbor communication is extremely fast, and large 3-D models are feasible because of the intrinsic parallelism of the conservation equations.

We investigate both finite difference and interpolation errors and attempt to determine whether or not anisotropy can be modeled precisely using local finite difference and interpolation operators. We derive the numerical dispersion relation for the homogeneous case for a staggered cartesian finite difference scheme using arbitrary convolution operators and time order. This allows us to determine the numerical phase and group velocity and compare them with analytical results. The resulting relations will enable accurate operators to be designed for general elastic models with arbitrary anisotropic symmetries.

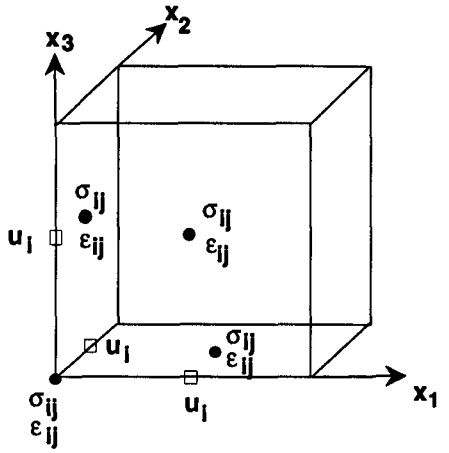

FIG. 1. Finite-difference grid cell. Stress, strain and displacement are defined at points allowing all fields to be calculated without interpolations.

THE ANISOTROPIC WAVE EQUATION

In this section, we recall the anisotropic elastic wave equation and present the time extrapolation algorithm. Subsequently, we introduce the spatial discretization along with the discrete derivative and interpolation operators that will be used to solve the wave equation.

The time extrapolation algorithm

Let $\rho(\mathbf{x})$ and $c_{ij}^{k\ell}(\mathbf{x})$, respectively, denote the density and the elastic stiffnesses at point $\mathbf{x}$ in an earth model. Furthermore, let $u_i(\mathbf{x}, t)$ and $\ddot{u}_i(\mathbf{x}, t)$ denote the ith component of displacement and acceleration at time t, and $\sigma_{ij}(\mathbf{x}, t)$ and $\varepsilon_{ij}(\mathbf{x}, t)$ represent the stress and strain tensors. The ith component of the body force source term is $f_i(\mathbf{x}, t)$. The time extrapolation problem is to calculate the components of the displacement $u_i(\mathbf{x}, t + \Delta t)$ from the *known* components of displacement at the previous timesteps ($u_i(\mathbf{x}, t)$, $u_i(\mathbf{x}, t - \Delta t)$, ...) for a given earth model. Using the summation convention that repeated, indices are summed when one index is an upper index and the other is a lower index and notation $\partial_i = \partial/\partial x_i$, the physics of elastic media in the small displacement limit is expressed using the strain-displacement relation

$$\varepsilon_{ij}(\mathbf{x}, t) = \tfrac{1}{2}(\partial_j u_i(\mathbf{x}, t) + \partial_i u_j(\mathbf{x}, t)), \qquad (1)$$

the stress-strain relation or the generalized Hooke's law,

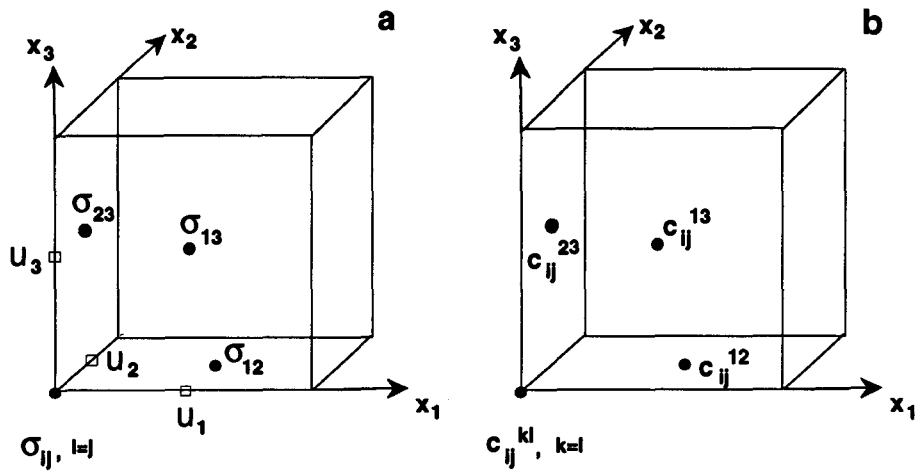

FIG. 2. (a) Location of the elements of the stress (and strain) tensor and the components of the displacement vector on the Cartesian grid cell. (b) Staggering of the elements of the elasticity tensor.

$$\sigma_{ij}(\mathbf{x}, t) = c_{ij}^{k\ell}(\mathbf{x})\varepsilon_{k\ell}(\mathbf{x}, t) + M_{ij}, \quad (2)$$

where M_{ij} is a moment tensor describing the source, and the linear momentum conservation equation,

$$\ddot{u}_i(\mathbf{x}, t) = \frac{1}{\rho(\mathbf{x})}\left(\partial^j \sigma_{ij}(\mathbf{x}, t) + f_i(\mathbf{x}, t)\right)$$

$$= L_i^{\ell} u_{\ell}(\mathbf{x}, t) + \frac{f_i(\mathbf{x}, t)}{\rho(\mathbf{x})}, \quad (3)$$

subject to the initial conditions,

$$\dot{u}_i(\mathbf{x}, 0) = 0, \qquad u_i(\mathbf{x}, 0) = 0, \quad (4)$$

where operator $L_i^{\ell} = (1/\rho(\mathbf{x}))\partial^j c_{ij}^{k\ell}\partial_k$.

The displacement may be extrapolated in time using a Taylor's expansion (Dablain, 1986)

$$u_i(\mathbf{x}, t + \Delta t) = 2u_i(\mathbf{x}, t) - u_i(\mathbf{x}, t - \Delta t)$$

$$+ 2\sum_{n=1}^{N} \frac{\Delta t^{2n}}{(2n)!} u_i^{(2n)}(\mathbf{x}, t), \quad (5)$$

where the wave equation (3) leads to the recursion

$$u_i^{(2n)}(\mathbf{x}, t) = \frac{\partial^{2n} u_i(\mathbf{x}, t)}{\partial t^{2n}} = L_i^{\ell} u_{\ell}^{(2n-2)}(\mathbf{x}, t)$$

$$+ f_i^{(2n-2)}(\mathbf{x}, t)/\rho(\mathbf{x}), \quad (6)$$

which is used to obtain the higher order time derivatives.

The partial derivative of a scalar field can be written as a convolution in a very general way. In a discretized version, the convolution is obtained as a convolution sum, as will be shown below.

The finite-difference algorithm to propagate elastic waves is implemented as

$$\dot{u}_i(\mathbf{x}, 0) = 0, \qquad u_i(\mathbf{x}, 0) = 0$$

for all time

$$[u_i(\mathbf{x}, t) \rightarrow \partial_j u_i(\mathbf{x}, t)$$

$$\partial_j u_i(\mathbf{x}, t) \rightarrow \varepsilon_{ij}(\mathbf{x}, t)$$

$$\varepsilon_{ij}(\mathbf{x}, t),\ c_{ij}^{k\ell}(\mathbf{x}, t) \rightarrow \sigma_{ij}(\mathbf{x}, t)$$

$$\sigma_{ij}(\mathbf{x}, t) \rightarrow \partial^j \sigma_{ij}(\mathbf{x}, t)$$

$$\rho(\mathbf{x}),\ \partial_j \sigma_{ij}(\mathbf{x}, t),\ f_i(\mathbf{x}, t) \rightarrow \ddot{u}_i(\mathbf{x}, t)$$

$$\ddot{u}_i(\mathbf{x}, t) \rightarrow \ddot{u}_i^{(2n-2)}(\mathbf{x}, t)$$

$$\ddot{u}_i^{(2n-2)}(\mathbf{x}, t) \rightarrow u_i(\mathbf{x}, t + \Delta t)].$$

The algorithm is implemented on a massively parallel computer (128 node CM5), so each variable is defined on the cartesian grid as a "parallel" variable.

GRID STAGGERING

All fields required to calculate the propagating wavefield are discretized. In a staggered grid, the fields are not defined at the same locations. A staggered grid is based on the idea of centering the derivative operators halfway between the grid points rather than on the grid points [for a 2-D example see Virieux (1986)]. This means one grid will contain the function values, e.g., the displacement, and a different grid will contain the function derivatives, e.g., stress. Such a scheme converges faster and results in improved accuracy.

Stress, strain and displacement

Figure 2 shows a cell of the staggered-grid scheme in three dimensions. Seven different locations are required to specify the stress, strain, and displacement components of the cell. While the diagonal elements of the stress and strain tensors are defined at the corner of the cell, the off-diagonal elements are located at the center of the cube faces.

Elastic tensor

To minimize the overall interpolation error, the elements of the elasticity tensor are staggered according to the indices describing the strains. Figure 2b shows the location of the elements of the tensor of elastic stiffnesses in the grid cell. The components of the displacement vector u_i are located half way between the corners of the cube.

Interpolations

Using a staggered grid implies that the off-diagonal elements of stress and strain tensors are not defined at the same location. When evaluating the stress-strain relation (Hooke's law), it is necessary to sum over a linear combination of the elements of the elasticity tensor and the elements of the strain tensor, for example

$$\sigma_{12} = c_{12}^{11}\varepsilon_{11} + c_{12}^{12}\varepsilon_{12} + \cdots + c_{12}^{32}\varepsilon_{32} + c_{12}^{33}\varepsilon_{33}. \quad (7)$$

If we determine the Hooke sum at the points where the diagonal elements of the stress are defined, the off-diagonal elements of the strain have to be interpolated to these locations and the off-diagonal elements of the stress tensor will have to be reinterpolated to their proper locations. The grid staggering may be represented using the unitary shift operators

$$D_{\vec{j}}(k) = e^{ik_j \Delta x_j/2}, \quad (8)$$

for a forward shift and

$$D_{\overleftarrow{j}}(k) = e^{-ik_j \Delta x_j/2} \quad (9)$$

for a backward shift along the jth axis. Note that the representation of equations (8) and (9) in the space domain are δ-functions centered at $\pm\Delta x_j/2$. For the rest of this paper, we denote the staggering of the fields, where it clarifies the interpolation, by an arrow above the indices. An off-diagonal strain element would thus read $\varepsilon_{ij}^{\vec{}}$ implying shifting by half a grid point along the ith and jth axis, and $\sigma_{ij}^{\vec{}}$ and $c_{ij}^{k\ell}$, respectively, denote the staggering of stress and elasticity tensor.

Note that this shifting can be interpreted as an exact interpolation, because given a sampling interval Δx, the evaluation of the discretized function $f(x_n)$, $x_n = n\Delta x$ at $x_n + \Delta x/2$ is done by a convolution of the function itself

with the exact interpolation operator. In the following section, the numerical interpolation operator will be derived as the band-limited representation of the shift operator.

THE OPERATORS

The most general way of writing an interpolation or derivative operator is as a convolution, e.g.,

$$\partial_x f(x) = \int_{-\infty}^{\infty} p(x-\chi) f(\chi)\, d\chi, \tag{10}$$

where $p(x)$ is the finite difference operator in the space domain. With spatial discretization the integral turns into a convolution sum. This description is general in the sense that it includes the case when the operator consists of two points only—a second order scheme—and also the case when all the points are used to calculate the derivative, as with Fourier methods.

Interpolation operator

In our finite difference scheme, we need to shift some elements of the strain and stress tensors at $\Delta x/2$. A shift of a function in the space domain corresponds to a multiplication in the wavenumber domain:

$$f\left(x+\frac{\Delta x}{2}\right) = \int_{-\infty}^{\infty} F(k) e^{ik(x+\Delta x/2)}\, dk.$$

Let the interpolation operator be denoted by

$$D_{\vec{x}}(k) = e^{ik\,\Delta x/2}. \tag{11}$$

A multiplication in the wavenumber domain corresponds to a convolution in the space domain. Thus,

$$f\left(x+\frac{\Delta x}{2}\right) = \int_{-\infty}^{\infty} D_{\vec{x}}(k) F(k) e^{ikx}\, dk \tag{12}$$

is equivalent to

$$f\left(x+\frac{\Delta x}{2}\right) = \int_{-\infty}^{\infty} d_{\vec{x}}(x-\chi) f(\chi)\, d\chi, \tag{13}$$

where

$$d_{\vec{x}}(x) = \mathcal{F}^{-1}\{D_{\vec{x}}(k)\}, \tag{14}$$

$\mathcal{F}^{-1}$ being the inverse Fourier transform.

When space is discretized, the wavenumber domain has upper bounds corresponding to the Nyquist wavenumber, and convolution expressed by the integral becomes a convolution sum

$$\tilde{f}\left(x_n+\frac{\Delta x}{2}\right) = \sum_{m=n-L/2}^{n+L/2-1} d_{\vec{x}}(x_n-\chi_m) f(\chi_m), \tag{15}$$

where the tilde denotes the approximate value of $f(x_n + \Delta x/2)$ and L is the length of the operator. The value is approximate because the convolution sum is finite ($L < \infty$). In the following, we will develop the analytic expression for the numerical interpolation operator in the space domain.

Because of discretization, the wavenumber domain is limited and, for example, the forward operator is

$$D_{\vec{x}}(k) = e^{ik\,\Delta x/2}[H(k+k^{\max}) - H(k-k^{\max})], \tag{16}$$

H being the Heaviside function with a representation in the space domain of

$$d_{\vec{x}}(x) = \frac{\sin\left(k^{\max}\left(x+\frac{\Delta x}{2}\right)\right)}{\pi\left(x+\frac{\Delta x}{2}\right)}. \tag{17}$$

Discretization using

$$\begin{cases} x_{n+1/2} = (n+\frac{1}{2})\Delta x \\ k^{\max} = \dfrac{\pi}{\Delta x} \end{cases} \tag{18}$$

leads to the discrete coefficients

$$d_{\vec{x}}(x_n) = \frac{(-1)^n}{\pi \Delta x (n+\frac{1}{2})}. \tag{19}$$

These coefficients should be tapered by a Gaussian to reduce edge effects, with

$$g(x_n) = e^{-\alpha((n-1/2)\Delta x)^2}, \tag{20}$$

α being a value to fix according to the number of points used for the convolution. For an eight-point operator we found that tapering using $\alpha = 0.2$ minimized the edge effects, and we denote the tapered truncated operator of length L as

$$\tilde{d}^L(x_n) = g(x_n) d_{\vec{j}}(x_n). \tag{21}$$

To perform the error analysis we compute the numerical interpolation operator in the wavenumber domain by a discrete Fourier transform

$$\tilde{D}^L_{\vec{j}} = \mathcal{F}\{\tilde{d}^L_{\vec{j}}\}, \tag{22}$$

where L is the number of points in the convolution operator.

The amplitude of the interpolation operator $\tilde{D}^L_{\vec{j}}$ for different lengths is compared with the exact operator $D_{\vec{j}}$ in Figure 3. The exact operator $|e^{ik_j \Delta x_j/2}| = 1$ is a box function spanning the interval $[-k_j^{\max}, k_j^{\max}]$. The more points used to calculate the interpolation, the closer the numerical operator is to the exact operator.

To demonstrate which operations are affected by the described interpolation, we determine the Hooke sum in the 3-D case. Denoting $d_{\vec{ij}}$ and $d_{\overleftarrow{ij}}$ as two subsequent forward and backward interpolations, respectively, we obtain for a diagonal stress element for example σ_{11}:

$$\sigma_{11} = c_{11}^{11}\varepsilon_{11} + d_{\overleftarrow{12}} c_{11}^{\vec{12}} \varepsilon_{\vec{12}} + \ldots d_{\overleftarrow{23}} c_{11}^{\vec{12}} \varepsilon_{\vec{12}} + \ldots c_{11}^{33}\varepsilon_{33}, \tag{23}$$

and for an off-diagonal element, e.g. $\sigma_{\vec{12}}$,

$$\sigma_{\vec{12}} = d_{\vec{12}} c_{11}^{12}\varepsilon_{11} + c_{12}^{\vec{12}}\varepsilon_{\vec{12}} + \ldots d_{\vec{12}} d_{\overleftarrow{23}} c_{12}^{\vec{23}} \varepsilon_{\vec{23}} + d_{\vec{12}} c_{12}^{33}\varepsilon_{33}, \tag{24}$$

illustrating the necessity for single and double interpolations of some of the strain elements. This analysis indicates that elements of the elasticity tensor are affected by the interpolations. In condensed notation 11 → 1,22 → 2,33 → 3,23 → 4,13 → 5,12 → 6, we obtain

$$c_{pq} = \begin{pmatrix} c_{11} & c_{12} & c_{13} & \hat{c}_{14} & \hat{c}_{15} & \hat{c}_{16} \\ c_{21} & c_{22} & c_{23} & \hat{c}_{24} & \hat{c}_{25} & \hat{c}_{26} \\ c_{31} & c_{32} & c_{33} & \hat{c}_{34} & \hat{c}_{35} & \hat{c}_{36} \\ \hat{c}_{41} & \hat{c}_{42} & \hat{c}_{43} & c_{44} & \hat{\hat{c}}_{45} & \hat{\hat{c}}_{46} \\ \hat{c}_{51} & \hat{c}_{52} & \hat{c}_{53} & \hat{\hat{c}}_{54} & c_{55} & \hat{\hat{c}}_{56} \\ \hat{c}_{61} & \hat{c}_{62} & \hat{c}_{63} & \hat{\hat{c}}_{64} & \hat{\hat{c}}_{65} & c_{66} \end{pmatrix}, \quad (25)$$

where the elements affected from single interpolation have been denoted by a hat and those affected by double interpolations by a double hat. This has important consequences regarding which elastic models will be affected the most by the interpolations. Comparing equation (25) with the representation of c_{pq} for different anisotropic symmetry systems (see Crampin, 1984), we notice the following. For symmetry systems higher than monoclinic (not more than nine independent elastic constants), there is no interpolation error when the axes of symmetry are aligned with the coordinate axes. It also means that whenever a cubic, hexagonal, orthorhombic or tetragonal(1) medium is oriented at an oblique angle to the coordinate axis, an interpolation error will be present. The error will be quantified in the section on numerical dispersion.

Space derivatives

In this section, we develop the derivative operator in the wavenumber and space domain in a manner similar to the development of the interpolation operator. A derivative with respect to the x-coordinate can be written as

$$\partial_x f(x) = \int_{-\infty}^{\infty} \partial_x F(k) e^{-ikx}\, dk,$$

$$= \int_{-\infty}^{\infty} -ikF(k) e^{-ikx}\, dk. \quad (26)$$

Denoting

$$P(k) = -ik, \quad (27)$$

so that

$$\partial_x f(x) = \int_{-\infty}^{\infty} P(k)F(k) e^{-ikx}\, dk. \quad (28)$$

we write the derivative as a convolution in the space domain

$$\partial_x f(x) = \int_{-\infty}^{\infty} p(x - \chi) f(\chi)\, d\chi, \quad (29)$$

which in the discrete and band-limited world turns into a convolution sum. We will now develop the analytic representation of $p(x)$.

The spatial discretization implies that frequencies are limited by a Nyquist frequency. This limitation can be expressed using the Heaviside function:

$$P(k) = ik[H(k + k^{\max}) - H(k - k^{\max})]. \quad (30)$$

Transforming back into the space domain yields

$$p(x) = \frac{1}{\pi x^2} [\sin(k^{\max}x) - k^{\max}x \cos(k^{\max}x)], \quad (31)$$

which is the derivative of a sinc function. The centered finite-difference derivatives are defined halfway between the grid points. We therefore discretize according to

$$\begin{cases} x_{n+1/2} (n + \frac{1}{2})\Delta x \\ k^{\max} = \dfrac{\pi}{\Delta x} \end{cases}, \quad (32)$$

leading to the following coefficients

$$p \vec{x} (x_n) = \frac{(-1)^n}{\pi((n + \frac{1}{2})\Delta x)^2}. \quad (33)$$

To reduce edge effects, these coefficients are tapered using a Gaussian function (see the section on the interpolation operator).

For the error analysis we can now represent the derivative operator in the wavenumber domain

$$\tilde{\vec{P}}_j^L = \mathcal{F}\{\vec{p}_j^L\}, \quad (34)$$

and determine the numerical wavenumber $\tilde{k}$ using equation (27)

$$\tilde{k}_j = i\tilde{\vec{P}}_j^L(\mathbf{k}), \quad (35)$$

which will be used to determine the numerical wave properties.

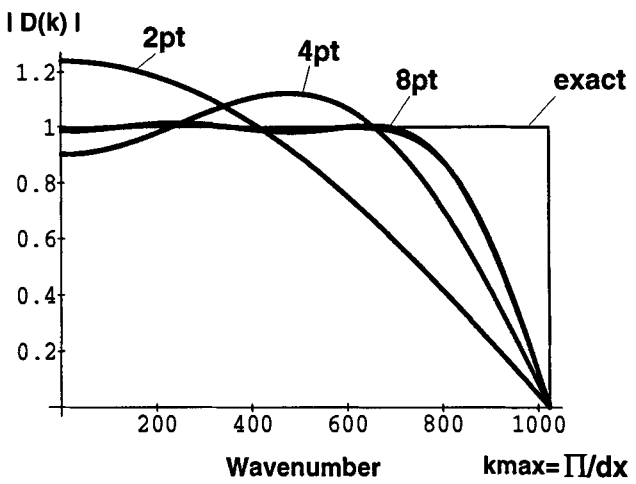

FIG. 3. The numerical interpolation operator in the wavenumber domain for different number of points used for the convolution compared with the exact operator.

Figure 4 shows the numerical derivative operator $\tilde{P}^{\frac{L}{j}}(k)$ and the exact operator $P^{\frac{}{j}}(k)$ as functions of wavenumber for different number of points L used for the convolution sum. Determination of the corresponding numerical frequency allows the numerical phase velocity to be calculated (see below).

In the above sections we developed the numerical interpolation and derivative operators that will be used in later sections to study the numerical dispersion relation. Note that these operators may be further optimized when, for example, frequencies are restricted to a known frequency band (e.g., Holberg, 1987). In this work we focus on the effect of anisotropy on the error in the wave properties.

THE DISPERSION RELATION

In this section, we extend the dispersion relation found by Crase (1990) for the 2-D case and by Rodrigues and Mora (1992) for the 3-D case to general elastic anisotropic 3-D media. The dispersion relation including the numerical operators for the space derivatives and interpolation is derived in the wavenumber domain. The numerical frequency will be determined as a function of numerical wavenumber and time increment Δt carefully chosen according to the stability limits. This allows us to determine the numerical phase and group velocity in any direction for a given wavenumber. The error in the phase and group velocities can be calculated and the operators may be optimized with respect to a particular elastic model.

For simplicity, we use the same notation for numerical and exact operators, unless stated otherwise. However, the fields in the wavenumber domain will be denoted by a hat.

In the space domain, the wave equation can be written as,

$$\frac{\partial^2 \mathbf{u}}{\partial t^2}(\mathbf{x}, t) = \underline{\mathbf{M}}\mathbf{u}(\mathbf{x}, t). \tag{36}$$

In the homogeneous isotropic case, the matrix $\underline{\mathbf{M}}$ can be written in a simple form,

$$\underline{\mathbf{M}} = \frac{1}{\rho(\mathbf{x})} * \begin{pmatrix} (\lambda + 2\mu)\partial_{xx}^2 + \mu(\partial_{yy}^2 + \partial_{zz}^2) & (\lambda + \mu)\partial_x\partial_y & (\lambda + \mu)\partial_x\partial_z \\ (\lambda + \mu)\partial_x\partial_y & (\lambda + 2\mu)\partial_{yy}^2 + \mu(\partial_{xx}^2 + \partial_{zz}^2) & (\lambda + \mu)\partial_y\partial_z \\ (\lambda + \mu)\partial_x\partial_z & (\lambda + \mu)\partial_y\partial_z & (\lambda + 2\mu)\partial_{zz}^2 + \mu(\partial_{xx}^2 + \partial_{yy}^2) \end{pmatrix}. \tag{37}$$

In the wavenumber domain the wave equation reads

$$\frac{\partial^2 \hat{\mathbf{u}}}{\partial t^2}(\mathbf{k}, t) = -\hat{\underline{\mathbf{M}}}\hat{\mathbf{u}}(\mathbf{k}, t), \tag{38}$$

where $\hat{\underline{\mathbf{M}}}$ for the isotropic case turns into

$$\hat{\underline{\mathbf{M}}} = \begin{pmatrix} c_p^2 k_x^2 + c_s^2(k_y^2 + k_z^2) & (c_p^2 - c_s^2)k_x k_y & (c_p^2 - c_s^2)k_x k_z \\ (c_p^2 - c_s^2)k_x k_y & c_p^2 k_y^2 + c_s^2(k_x^2 + k_z^2) & (c_p^2 - c_s^2)k_y k_z \\ (c_p^2 - c_s^2)k_x k_z & (c_p^2 - c_s^2)k_y k_z & c_p^2 k_z^2 + c_s^2(k_x^2 + k_y^2) \end{pmatrix}, \tag{39}$$

where c_p and c_s are the isotropic P- and S-wave velocities, respectively. In the following, the eigenvalues of the matrix $\hat{\underline{\mathbf{M}}}$ will be required. Therefore, we write equation (38) as

$$\frac{\partial^2 \hat{\mathbf{u}}}{\partial t^2}(\mathbf{k}, t) = -\hat{\underline{\mathbf{V}}}\hat{\underline{\mathbf{\Lambda}}}\hat{\underline{\mathbf{V}}}^T\hat{\mathbf{u}}(\mathbf{k}, t), \tag{40}$$

where $\hat{\underline{\mathbf{\Lambda}}}$ contains the eigenvalues of $\hat{\underline{\mathbf{M}}}$ and $\hat{\underline{\mathbf{V}}}$, its eigenvectors. In the isotropic case the eigenvalues can be given as

$$\hat{\underline{\mathbf{\Lambda}}} = \begin{pmatrix} c_p^2(k_x^2 + k_y^2 + k_z^2) & 0 & 0 \\ 0 & c_s^2(k_x^2 + k_y^2 + k_z^2) & 0 \\ 0 & 0 & c_s^2(k_x^2 + k_y^2 + k_z^2) \end{pmatrix}. \tag{41}$$

Note that

$$\hat{\underline{\mathbf{M}}}^n = (\hat{\underline{\mathbf{V}}}\hat{\underline{\mathbf{\Lambda}}}\hat{\underline{\mathbf{V}}}^T)^n = \hat{\underline{\mathbf{V}}}\hat{\underline{\mathbf{\Lambda}}}^n\hat{\underline{\mathbf{V}}}^T. \tag{42}$$

In the anisotropic case, it is no longer concise to write explicit expressions for the eigenvalues of the matrix $\hat{\underline{\mathbf{\Lambda}}}$ because of the more complicated form of matrix $\hat{\underline{\mathbf{M}}}$. A convenient way to write $\hat{\underline{\mathbf{M}}}$ is by introducing the matrices $\underline{\mathbf{A}}$, $\underline{\mathbf{B}}$, $\underline{\mathbf{C}}$, $\underline{\mathbf{D}}$, $\underline{\mathbf{E}}$, $\underline{\mathbf{F}}$ in the form

$$\underline{\mathbf{A}} = \begin{pmatrix} c_{11} & d_{\vec{1}2}c_{16} & d_{\vec{1}3}c_{15} \\ d_{\vec{1}2}c_{16} & c_{66} & d_{\vec{1}3}d_{\vec{1}2}c_{65} \\ d_{\vec{1}3}c_{15} & d_{\vec{1}2}d_{\vec{1}3}c_{65} & c_{55} \end{pmatrix},$$

$$\underline{\mathbf{B}} = \begin{pmatrix} d_{\vec{1}2}c_{16} & c_{12} & d_{\vec{1}3}d_{\vec{1}2}c_{56} \\ c_{66} & d_{\vec{1}2}c_{62} & d_{\vec{1}3}c_{52} \\ d_{\vec{2}3}c_{14} & d_{\vec{1}2}d_{\vec{2}3}c_{64} & d_{\vec{1}3}d_{\vec{2}3}c_{54} \end{pmatrix},$$

$$\underline{\mathbf{C}} = \begin{pmatrix} d_{\vec{1}3}c_{15} & d_{\vec{1}2}d_{\vec{1}3}c_{65} & c_{55} \\ d_{\vec{2}3}c_{14} & d_{\vec{1}2}d_{\vec{2}3}c_{64} & d_{\vec{1}3}d_{\vec{2}3}c_{54} \\ c_{13} & d_{\vec{1}2}c_{63} & d_{\vec{1}3}c_{53} \end{pmatrix},$$

$$\underline{\mathbf{D}} = \begin{pmatrix} c_{66} & d_{\vec{1}2}c_{62} & d_{\vec{2}3}d_{\vec{1}2}c_{64} \\ d_{\vec{1}2}c_{62} & c_{22} & d_{\vec{2}3}c_{24} \\ d_{\vec{1}2}d_{\vec{2}3}c_{64} & d_{\vec{2}3}c_{24} & c_{44} \end{pmatrix},$$

$$\underline{\mathbf{E}} = \begin{pmatrix} d_{\vec{1}2}d_{\vec{1}3}c_{65} & d_{\vec{1}3}c_{25} & d_{\vec{2}3}d_{\vec{1}3}c_{45} \\ d_{\vec{1}2}d_{\vec{2}3}c_{64} & d_{\vec{2}3}c_{24} & c_{44} \\ d_{\vec{1}2}c_{63} & c_{23} & d_{\vec{2}3}c_{43} \end{pmatrix},$$

$$\underline{\mathbf{F}} = \begin{pmatrix} c_{55} & d_{\vec{2}3}d_{\vec{1}3}c_{54} & d_{\vec{1}3}c_{54} \\ d_{\vec{1}3}d_{\vec{2}3}c_{54} & c_{44} & d_{\vec{2}3}c_{43} \\ d_{\vec{1}3}c_{53} & d_{\vec{2}3}c_{43} & c_{33} \end{pmatrix}, \tag{43}$$

having a corresponding representation in the wavenumber domain. Then, using the above definition of successive interpolations, we can write

$$\hat{\underline{\mathbf{M}}} = \begin{pmatrix} \mathbf{k}\hat{\underline{\mathbf{A}}}\mathbf{k}^T & \mathbf{k}\hat{\underline{\mathbf{B}}}\mathbf{k}^T & \mathbf{k}\hat{\underline{\mathbf{C}}}\mathbf{k}^T \\ \mathbf{k}\hat{\underline{\mathbf{B}}}\mathbf{k}^T & \mathbf{k}\hat{\underline{\mathbf{D}}}\mathbf{k}^T & \mathbf{k}\hat{\underline{\mathbf{E}}}\mathbf{k}^T \\ \mathbf{k}\hat{\underline{\mathbf{C}}}\mathbf{k}^T & \mathbf{k}\hat{\underline{\mathbf{E}}}\mathbf{k}^T & \mathbf{k}\hat{\underline{\mathbf{F}}}\mathbf{k}^T \end{pmatrix}, \tag{44}$$

where $\mathbf{k}$ is the wavenumber vector and $\mathbf{k}^T$ its transpose. Note that the elements of matrix $\hat{\underline{\mathbf{M}}}$ are scalars. It turns out that only the modulus of the interpolation operator is needed in the expressions (43). The matrix $\hat{\underline{\mathbf{M}}}$ is real, symmetric, and positive definite. This means that $\hat{\underline{\mathbf{M}}}$ has three positive eigenvalues.

For the error analysis of our finite difference scheme, we replace $\mathbf{k}$ with the numerical wavenumber $\tilde{\mathbf{k}}$ from equation (35) and the numerical interpolation operator from equation (22).

We can now develop the dispersion equation for our numerical scheme and express the frequency as a function of the wavenumber $\mathbf{k}$, the eigenvalues of matrix $\hat{\underline{\mathbf{M}}}$, $\lambda_k(\mathbf{k})$, and the order of the time extrapolation N as

$$\tilde{\omega}(\mathbf{k}, \Delta t) = \frac{2}{\Delta t} \arcsin \sqrt{-\frac{1}{2} \sum_{n=1}^{N} (-1)^n \lambda_i^{2n}(\mathbf{k}) \frac{\Delta t^{2n}}{(2n)!}}. \tag{45}$$

A more detailed derivation of equation (45) can be found in the Appendix. Equation (45) places constraints on the choice of the parameters Δt and Δx for given maximum propagation speeds and spatial operators. In the isotropic case, this is usually expressed by the stability criterion

$$\frac{c_p \Delta t}{\Delta x} \leq \varepsilon, \tag{46}$$

where c_p is the isotropic P-wave velocity and ε some value depending on the particular spatial operators. Rodrigues and Mora (1992) evaluated ε for different spatial and temporal orders. Table 1 shows the stability values for eight-point convolution operators and different temporal orders. The right side of Table 1 shows the coefficients of the symmetric interpolation and the antisymmetric derivative operator we used in the numerical examples below. Note that these coefficients have been optimized to give small errors below 60% Nyquist wavenumber. Other coefficients may be more accurate for higher wavenumbers but less accurate for low wavenumbers (see Holberg, 1987, for examples).

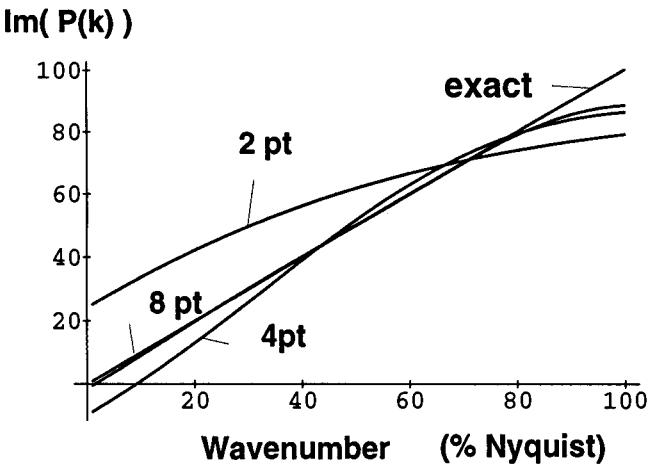

FIG. 4. Comparison of the numerical with the analytical derivative operator for different convolution operators, using 2, 4, and 8 points to calculate the derivative.

In the anisotropic case, a good first approximation can be made by replacing c_p in equation (46) by the maximum phase velocity of the anisotropic medium. In practice, the left-hand side of equation (46) should typically be less than 50% of its maximum value to obtain precise results. For a more detailed discussion on the stability properties of this scheme we refer to Rodrigues and Mora (1992).

It is now possible to determine the numerical phase velocity of the three wave types propagating in any direction through an anisotropic medium. Considering that the spatial discretization is not isotropic, the error depends on the direction of propagation. In this paper, we will stress the effect of the interpolation on wave propagation through generally anisotropic media. In the following sections, we compare analytical and numerical wave properties of anisotropic media.

THE NUMERICAL WAVE PROPERTIES

The numerical dispersion relation obtained in previous sections is used to study the error between the numerical group and phase velocities for an extremely anisotropic material. Since we are particularly interested in the effect of the interpolation on the wave properties for anisotropic material, we will separate this effect by comparing the following two cases. First, we determine the phase and group velocity for the staggered scheme. Second, we replace the numerical interpolation by the exact shift operator to omit the error caused by interpolation. This corresponds to the case when the elements of the stress and strain tensors are known at all locations in the grid cell shown in Figure 2. As Holberg (1987) already noticed, the peak error of the group velocity may be one order of magnitude larger than the maximum phase velocity error. It seems that it is sufficient to consider only the group velocity error. However, we are particularly interested in the anisotropic behavior of the error since we want to be able to distinguish between physical and numerical anisotropy. To understand the behavior of the numerical group velocity, it is necessary to consider the phase velocity. It is the phase error that is responsible for the spatial variation of the group error. Therefore we choose to show both the phase and the group velocity error.

The anisotropic material

The material under investigation was a medium without symmetry, (i.e., thus triclinic). This material has no physical

Table 1. Left: Stability factors ε for eight-point convolutions. N is the order of the time extrapolation. Right: Coefficients of interpolation ($p_{\vec{j}}$) and derivative ($d_{\vec{j}}$) operators for a convolution where $L = 8$ (the second half are obtained by symmetry and antisymmetry). Note that these results were obtained for $\Delta x = 1$.

N	ε	n	$d_{\vec{j}}$	$p_{\vec{j}}$
1	0.423	−3	−0.00784803	−0.00224229
2	0.733	−2	0.03647890	0.01459160
3	0.582	−1	−0.13530900	−0.09020590
4	0.981	0	0.60557100	1.21114000

significance; however, it displays a very strong anisotropy and allows us to study the limits of our approach. The elastic constants for the triclinic medium are

$$c_{\text{tri}} = \begin{pmatrix} 10.0 & 3.5 & 2.5 & -5.0 & 0.1 & 0.3 \\ 3.5 & 8.0 & 1.5 & 0.2 & -0.1 & -0.15 \\ 2.5 & 1.5 & 6.0 & 1.0 & 0.4 & 0.24 \\ -5.0 & 0.2 & 1.0 & 5.0 & 0.35 & 0.525 \\ 0.1 & -0.1 & 0.4 & 0.35 & 4.0 & -1.0 \\ 0.3 & -0.15 & 0.24 & 0.525 & -1.0 & 3.0 \end{pmatrix}, \tag{47}$$

the phase velocity variations for a material with density 1.0 g/cm^3 in the xz-plane being shown in Figure 5. The factor 10^{11} dyne cm^{-2} was omitted here. Note that for this material, it is not appropriate to speak of quasilongitudinal or quasitransverse waves. The medium is so strongly anisotropic that the polarizations are no longer approximately perpendicular or parallel to the direction of propagation. Also, the outer phase velocity sheet connects with the inner sheets. That means, that in some directions, the two faster wave types have the same phase velocities. Nevertheless, to simplify notation we denote the three phase velocities qP, $qS1$, and $qS2$, because of the decreasing eigenvalues of the Christoffel matrix, referring to the case of weak anisotropy.

Phase velocity error

In our example, we kept the parameters of the spatial operators constant and varied the wavenumber. This is equivalent to using different number of points per wavelength. Thus, 30 and 70% of the Nyquist wavenumber would correspond to approximately 6.7 and 2.9 points per wavelength, respectively. The spatial operators to compute derivatives and the interpolations were both calculated using an eight-point convolution; the coefficients being calculated by the above described methods. The time increment is chosen so that the calculations were at about 20% of the stability limit. For a maximum phase velocity of 2 km/s, $\Delta x = 20$ m, this would correspond to a time increment Δt of approximately 1.5 ms. We used a fourth-order time extrapolation scheme for the numerical examples below. The following numerical calculations have been done with Mathematica™.

Figure 6 shows the relative error of the three wave types to be at 70% Nyquist. The maximum errors are 2, 3, and 7% for qP, $qS1$, and $qS2$, respectively. The large error is mainly caused by the interpolation. This can be seen in the 2-D cut in Figure 7. The left column represents the spatial variation of the error at 30%, and the right column at 70% Nyquist. The dashed lines correspond to the case with exact interpolation; the solid lines represent the case with numerical interpolation. In all cases the numerical interpolation increases the maximum error.

The wave type that is the most affected is $qS2$. The maximum errors seem to coincide with extremal features of the phase velocity surface. Figure 8 summarizes the results for the material with triclinic symmetry. Below 50% Nyquist, the phase velocity error is smaller than 0.5%. The interpolation affects the results strongly for wavenumbers higher than 50% Nyquist.

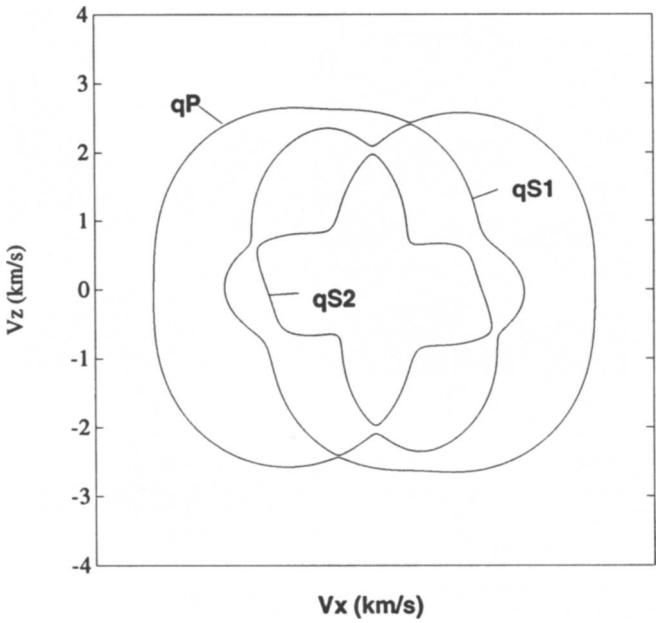

FIG. 5. Phase-velocity variations in the xz-plane for a material with triclinic symmetry. Same scaling on both axes.

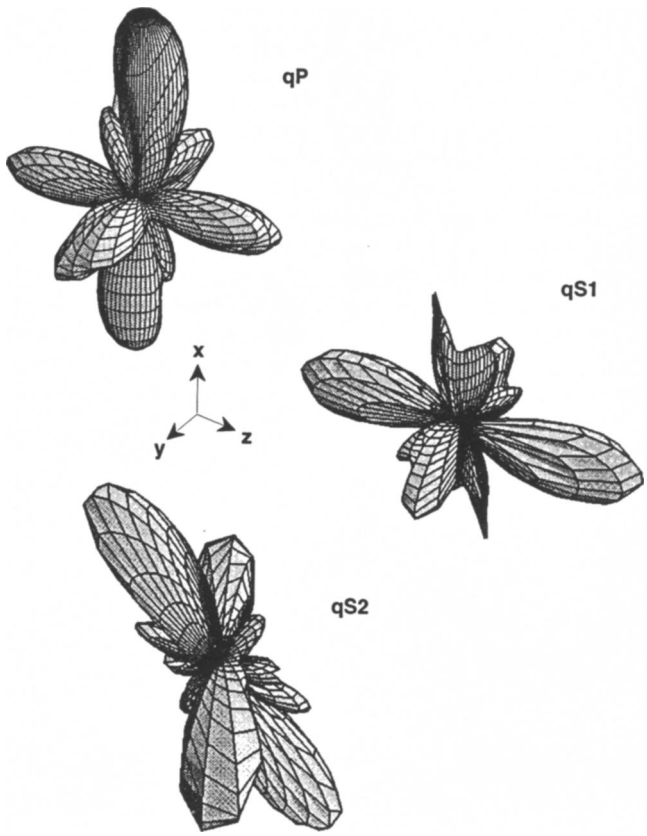

FIG. 6. The spatial variation of the relative error of the phase velocity at 70% Nyquist. The medium has triclinic symmetry. The maximum error for the three quasi waves are 2, 3, and 7% for qP, $qS1$, and $qS2$, respectively. Note that the maximum error of all three wave types is below 0.5% for wavenumbers up to 50% Nyquist.

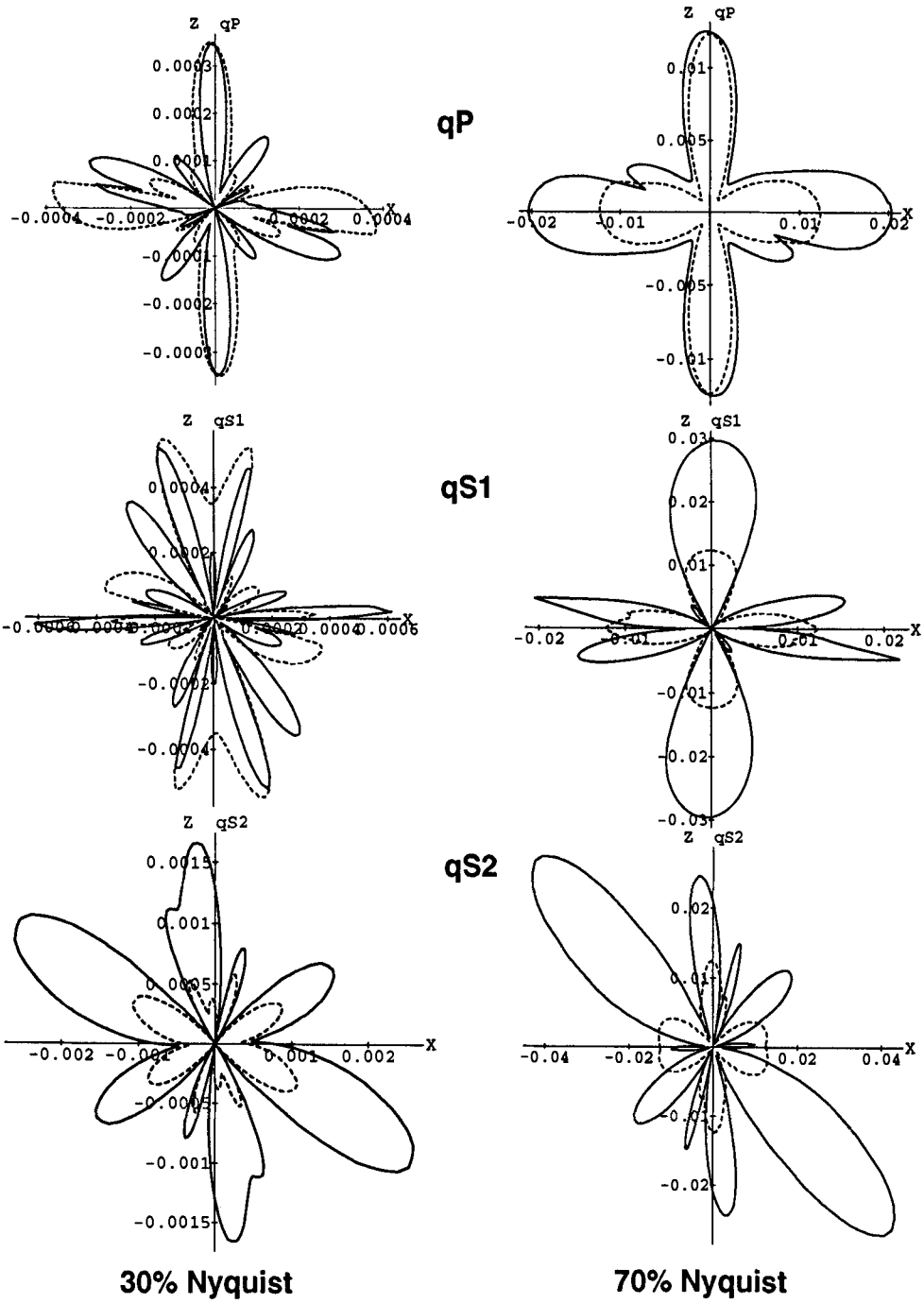

FIG. 7. The relative error of the phase velocity in the xz-plane for different wavenumbers. The medium has triclinic symmetry. The solid lines represent the case with numerical interpolation, the dashed lines the case with exact interpolation.

Group velocity error

What we observe in nature when recording high-frequency seismic waveforms is the velocity of the energy, i.e., the group velocity. It is therefore clear that we must focus on the effect of the numerical scheme on the group velocity. In addition, it is well known that in finite difference schemes, the group velocity error in finite difference schemes may be considerably larger than the phase velocity error. The group velocity $g(\mathbf{k})$ is the gradient of the frequency surface

$$g_i(\mathbf{k}) = \frac{\partial \omega(\mathbf{k})}{\partial k_i}. \tag{48}$$

Considering equation (48), it is evident that the numerical interpolation will have a large effect on the group velocity when the *shape* of the phase velocity sheet is affected by the interpolation. Note that in the plots showing the group velocity, we display the projection of the group velocity vector on the xz-plane, corresponding to a particular phase propagation direction in the xz-plane. This is not a cut through the wave surface and cannot be compared directly with snapshots.

The group velocity variations of the triclinic medium are shown in Figure 9. Because of the complexity of the phase velocity surface there is a large number of cusps.

Looking at the relative error of the group velocity in the xz-plane (Figure 10), we see that the effect of the numerical interpolation is large for this strongly anisotropic medium. In addition, we can see some directions in which the error exhibits sharp maxima. These directions may correspond to cuspoidal features, where small errors of the wavenumber lead to large changes in the direction of propagation. The error with numerical interpolation is larger than the error with exact interpolation for all wave types and the whole wavenumber range. It is larger than the phase velocity error, but for wavenumbers below 40% Nyquist, the error is smaller than 0.7%. This can be seen in Figure 11 where the maximum error is shown for all wavenumbers. The effect of the numerical interpolation is strongest for $qS2$. This may be because the $qS2$ is the most anisotropic of the three wave types. The fastest wave type (qP) is hardly affected by the interpolation, even for this strongly anisotropic case.

DISCUSSION

Finite-difference approximations to the wave equation are currently the most promising approach for large scale 3-D modeling of seismic-wave propagation in highly heterogeneous earth models. The researcher who is confronted with the question of which type of finite difference approach to

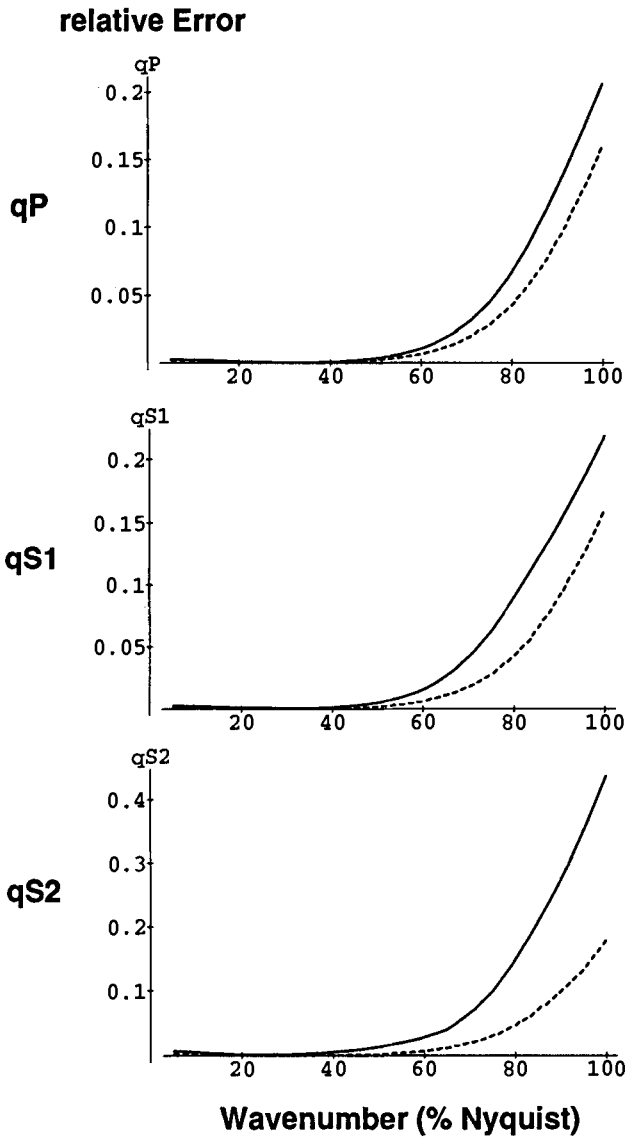

FIG. 8. The maximum phase velocity error in the whole wavenumber range. Triclinic symmetry. Dashed lines: exact interpolation operator; solid lines: numerical interpolation operator.

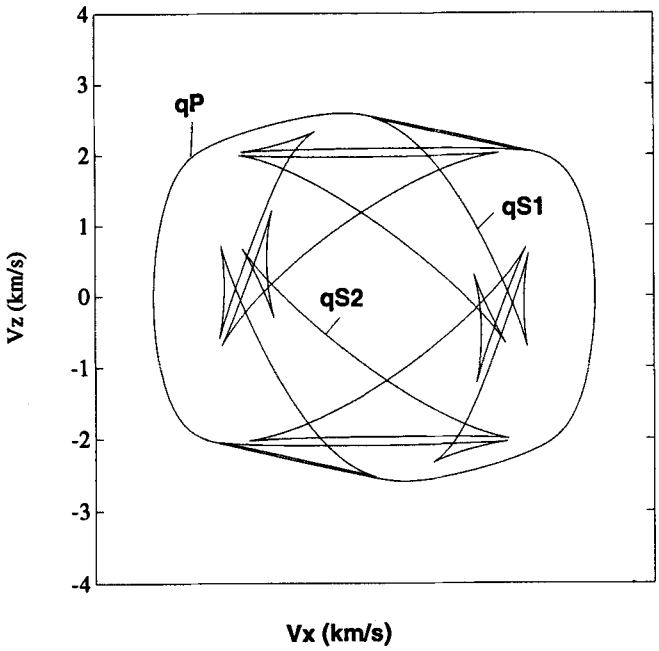

FIG. 9. Group velocity variations in the xz-plane for the case with triclinic symmetry. Note that projections of the group velocity vector are shown (see text). Both axes have the same scaling.

use is faced with a large number of publications and the same number of different ways of doing it. Two main streams could be noted. First, the pseudospectral methods developed in Kossloff and Baysal (1982), Kossloff et al. (1984), Kossloff and Kessler (1989), and Kossloff et al. (1990). In pseudospectral methods the derivatives of the fields are evaluated in the wavenumber domain. Second, the staggered-grid convolution methods of Mora (1989), Crase (1990), and Rodrigues and Mora (1992), which extend the work of Virieux (1986) to more precise operators for the space derivatives using band limited convolution operators obtained by representing the derivative operators in the wavenumber domain. The pseudospectral methods have been used in the general anisotropic case in Carcione et al. (1988, 1992) and Tessmer and Behle (1992), while the methods for staggered grids for anisotropic media were applied in Igel et al. (1991), and Leary et al. (1993). Triangular (in 2-D) or "minimal" (in *N-D*) grids for the spatial discretization were introduced in Magnier et al. (1994) that are both memory efficient and do not require interpolations during the

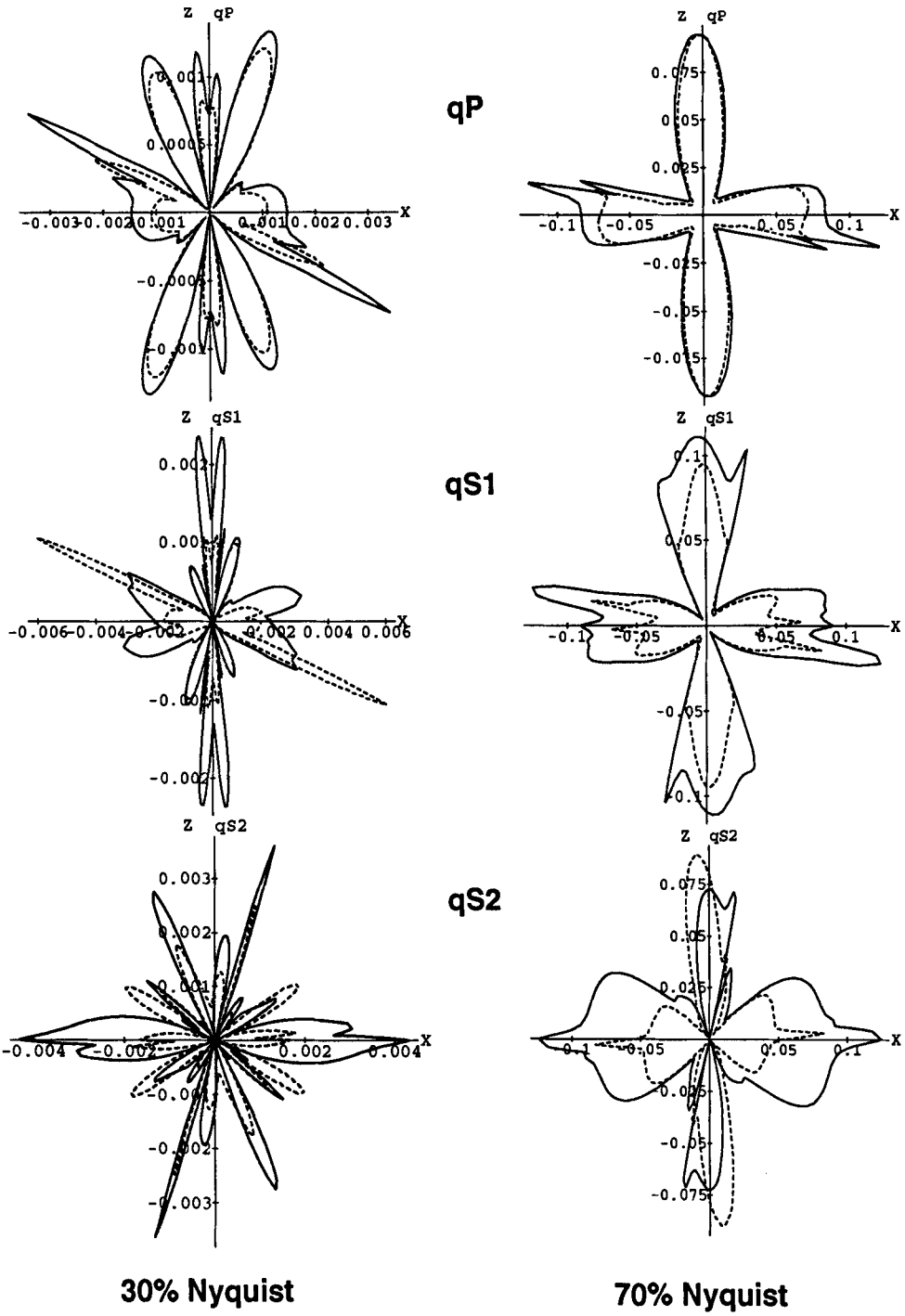

FIG. 10. The relative error of the group velocity in the xz-plane for different wavenumbers. The medium has triclinic symmetry. The solid lines represent the case with numerical interpolation, the dashed lines the case with exact interpolation.

calculation of the Hooke sum. While this discretization would eliminate the additional error caused by the interpolations required by the Cartesian scheme, numerical anisotropy will remain because of the (minimal) spatial discretization. Such anisotropic errors have not yet been analyzed but are expected to be of a similar magnitude to the error in the Cartesian scheme using exact interpolations but with different symmetry properties reflecting the different discretization.

In this paper, we investigated the feasibility of staggered finite difference schemes to model general material anisotropy. In staggered grids, numerical interpolations are required when the medium has certain types of anisotropic symmetry systems. We developed the numerical dispersion relation for our scheme and studied the effect of the interpolation on cases with arbitrary symmetry systems and strong anisotropy.

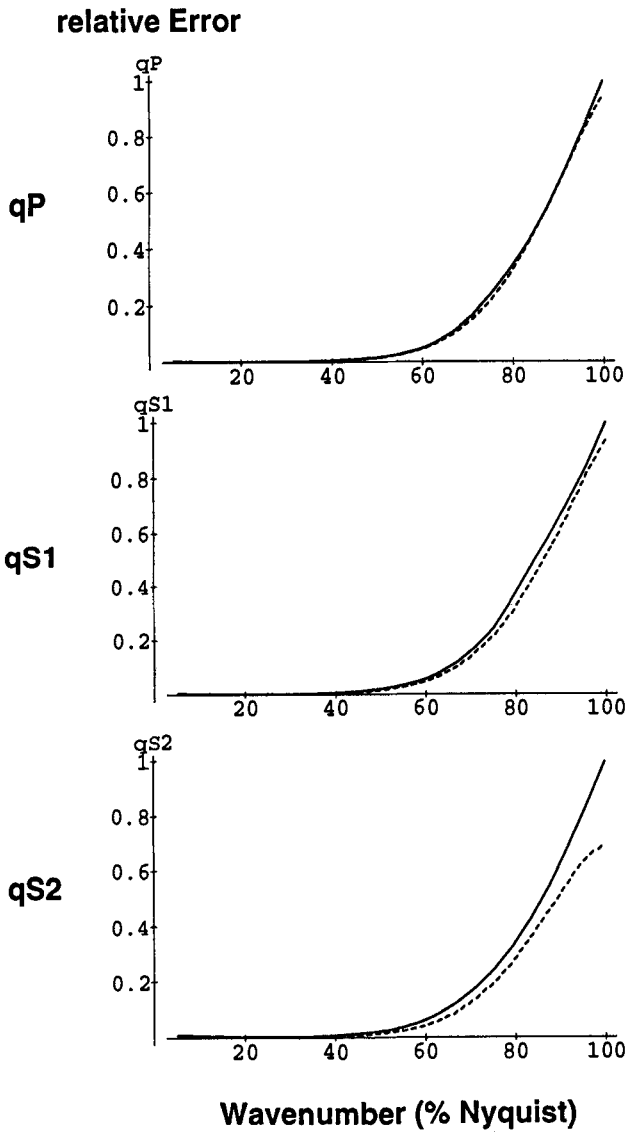

FIG. 11. The maximum group velocity error in the whole wavenumber range for the case with triclinic symmetry. Dashed lines: exact interpolation operator; solid lines: numerical interpolation operator.

The numerical experiment following the theoretical developments of the first sections are summarized in Table 2. We added the results of a second numerical experiment for a material of hexagonal symmetry with a symmetry axis at an oblique angle with respect to the coordinate axis.

From Table 2 and the previous considerations we can make the following general observations for the eight-point operator:

1) The error of the wave properties in the general anisotropic case for staggered finite difference grids depends on the length of the operator, the symmetry system of the anisotropic medium, the orientation of the symmetry axis with respect to the coordinate axis, and the degree of anisotropy.
2) The error resulting from the interpolation required for staggered grids is negligible in the case of weak anisotropy. When anisotropy is strong, the numerical interpolation may lead to substantial additional errors for wavenumbers close to Nyquist. However, for wavenumbers below 50% Nyquist (more than four points per wavelength) the *numerical* anisotropy induced by the spatial operators is orders of magnitude below the *physical* anisotropy, even for the case of strong anisotropy.
3) Numerical experiments show that general anisotropy can be modeled with high accuracy when a minimum number of points per wavelength ($\approx$4) is guaranteed.

It is clearly desirable to analyze the heterogeneous scheme and apply it to different types of models. These are our current research topics.

ACKNOWLEDGMENTS

This research has been funded in part by the French Ministry of National Education (MEN) and the National Center for Scientific Research (CNRS). It could not have been done without the help of the Sponsors of the Seismic Simulation Project (Amoco, CEA [French Atomic Energy Authority], Shell, Delany Enterprises Inc., Digital Equipment, Elf, GOCAD, Inverse Theory & Applications, Norsk Hydro, Unocal, Thinking Machines Co., and Total-CFP). We are grateful to the Centre National de Calcul Parallèle en Science de la Terre for allowing us to implement our

Table 2. The maximum error (in %) of the group velocity *qP*, *qS1*, *qS2* for different wavenumbers. The horizontal axis is the wavenumber in % Nyquist.

	20%	40%	60%	80%	100%
Hexagonal symmetry (10% anis.)					
qP	0.20	0.47	0.46	32	100
qS1	0.20	0.50	0.48	32	100
qS2	0.20	0.45	0.44	31	100
Triclinic symmetry (50% anis.)					
qP	0.20	0.56	4.7	34	100
qS1	0.20	0.51	4.8	33	100
qS2	0.34	0.79	6.0	34	100

algorithm on the Connection Machine CM-5 funded by the French Ministry of Education and Research. Thanks to Jean Virieux, Cord Jastram, Ekkehart Tessmer, Dominique Rodrigues, Joe Dellinger, David W. Eaton, Albert Tarantola, and one anonymous reviewer for critical comments.

REFERENCES

Carcione, J. M., Kossloff, D., Behle, A., and Seriani, G., 1992, A spectral scheme for wave propagation simulation in 3-D elastic anisotropic media: Geophysics, **57**, 1593–1607.

Carcione, J. M., Kossloff, D., Kossloff, R., 1988, Wave propagation simulation in an elastic anisotropic (transversely isotropic) solid, Part 3: Q. J. Mech. Appl. Math., **41**, 319–345.

Crampin, S., 1984, An introduction to wave propagation in anisotropic media: Geophys. J. Roy. Astr. Soc., **76**, 17–28.

Crase, E., 1990, High order (space and time) finite-difference modeling of the elastic wave equation: 60th Ann. Internat. Mtg., Soc. Expl. Geophys., Expanded Abstracts, 987–991.

Dablain, M., 1986, The application of high-order differencing to the scalar wave equation: Geophysics, **51**, 54–66.

Holberg, O., 1987, Computational aspects of the choice of operator and sampling interval for numerical differentiation in large-scale simulation of wave phenomena: Geophys. Prosp., **35**, 629–655.

Igel, H., Mora, P., and Rodrigues, D., 1991, 3-D wave propagation using finite-differences: 61st Ann. Internat. Mtg., Soc. Expl. Geophys., Expanded Abstracts, 1577–1579.

Kossloff, D., and Baysal, E., 1982, Forward modeling by a Fourier method: Geophysics, **47**, 1402–1412.

Kossloff, D., and Kessler, D., 1989. Seismic numerical modeling in oceanographic and geophysical tomography, *in* Desaubies, Y., Tarantola, A., and Zinn Justin, J., Eds., Session XL of the summer school of theoretical physics, Les Houches: Elsevier Science Publ.

Kossloff, D., Kessler, D., Filho, A. Q., Tessmer, E., Behle, A. and Strahilevitz, R., 1990, Solution of the equations of dynamic elasticity by a Chebyshev spectral method: Geophysics, **55**, 734–748.

Kossloff, D., Reshef, M., and Loewenthal, D., 1984, Elastic wave calculations by the Fourier method: Bull. Seis. Soc. Am., **74**, 875–891.

Leary, P., Igel, H. P., Mora, P., and Rodrigues, D., 1993, Finite-difference simulation of trapped wave propagation in fracture anisotropic low velocity layers: Can. J. Expl. Geoph., in print.

Magnier, S. A., Mora, P., and Tarantola, A., 1994, Finite differences on minimal grids, Geophysics, **59**, 1435–1443.

Mora, P., 1989, Modeling anisotropic waves in 3-D: 59th Ann. Internat. Mtg., Soc. Expl. Geophys., Expanded Abstracts, 1039–1043.

Reshef, M., Kosloff, D., Edwards, M., and Hsiung, C., 1988, Three-dimensional elastic modeling by the Fourier method: Geophysics, **53**, 1184–1193.

Rodrigues, D., and Mora, P., 1992, Analysis of a finite-difference solution to the three-dimensional elastic wave equation: 62nd Ann. Internat. Mtg., Soc. Expl. Geophys., Expanded Abstracts, 1247–1249.

Tessmer, E., and Behle, A., 1992, 3-D seismic modeling of general material anisotropy in the presence of the free surface by a Chebyshev spectral method: Technical Program, 54th Ann. Internat. Mtg., Europ. Assoc. Expl. Geoph., 134–135.

Virieux, J., 1986, *P-SV* wave propagation in heterogeneous media: Velocity-stress finite-difference method: Geophysics, **51**, 889–901.

APPENDIX

THE DISPERSION RELATION

In this appendix we derive the dispersion relation, starting from the representation of the time extrapolation as a Taylor expansion.

In the continuous world, the dynamics of the elastic system is expressed in terms of partial derivatives with respect to time. By contrast, the discrete dynamics is expressed through a Taylor expansion that enables the wavefield to be extrapolated by a time increment Δt. Using the notation in the body of the article, the extrapolation is given by

$$u_i(\mathbf{x}, t + \Delta t) = 2u_i(\mathbf{x}, t) - u_i(\mathbf{x}, t - \Delta t) + 2 \sum_{n=1}^{N} \frac{\Delta t^{2n}}{(2n)!} u_i^{(2n)}(\mathbf{x}, t), \quad \text{(A-1)}$$

or equivalently, in the wavenumber domain,

$$\hat{u}_i(\mathbf{k}, t + \Delta t) = 2\hat{u}_i(\mathbf{k}, t) - \hat{u}_i(\mathbf{k}, t - \Delta t) + 2 \sum_{n=1}^{N} \frac{\Delta t^{2n}}{(2n)!} \frac{\partial^{2n} \hat{u}_i}{\partial t^{2n}}(\mathbf{k}, t). \quad \text{(A-2)}$$

Replacing $\partial^{2n}\hat{u}_i/\partial t^{2n}(\mathbf{k}, t)$ by the rhs of equation (40) and making use of equation (42), we obtain

$$\hat{u}_i(\mathbf{k}, t + \Delta t) = 2\hat{u}_i(\mathbf{k}, t) - \hat{u}_i(\mathbf{k}, t - \Delta t) + 2\hat{\underline{\mathbf{V}}}\left(\sum_{n=1}^{N} (-1)^n \frac{\Delta t^{2n}}{(2n)!} \hat{\underline{\Lambda}}^n \right) \hat{\underline{\mathbf{V}}}^T \hat{u}_i(\mathbf{k}, t). \quad \text{(A-3)}$$

Transforming this equation to the frequency domain using

$$\int u(t \pm \Delta t) e^{i\omega t}\, dt = \int u(\tau) e^{i\omega(\tau \mp \Delta\tau)}\, d\tau = \hat{u}(\omega) e^{i \mp \omega \Delta t}, \quad \text{(A-4)}$$

yields

$$\hat{\mathbf{u}}(\mathbf{k}, \omega) e^{-i\omega\Delta t} = 2\hat{\mathbf{u}}(\mathbf{k}, \omega) - \hat{\mathbf{u}}(\mathbf{k}, \omega) e^{i\omega\Delta t} + 2\hat{\underline{\mathbf{V}}}\left(\sum_{n=1}^{N} (-1)^n \frac{\Delta t^{2n}}{(2n)!} \hat{\underline{\Lambda}}^n \right) \hat{\underline{\mathbf{V}}}^T \hat{\mathbf{u}}(\mathbf{k}, \omega). \quad \text{(A-5)}$$

This can be written as

$$0 = \hat{\underline{\mathbf{V}}} \left[\sin^2\left(\frac{\omega\Delta t}{2} \right) \hat{\underline{\mathbf{I}}} + \frac{1}{2} \left(\sum_{n=1}^{N} (-1)^n \frac{\Delta t^{2n}}{(2n)!} \hat{\underline{\Lambda}}^n \right) \right] \hat{\underline{\mathbf{V}}}^T \hat{\mathbf{u}}(\mathbf{k}, \omega),$$

or in a compact notation

$$0 = \hat{\underline{\mathbf{V}}} \hat{\underline{\mathbf{Q}}} \hat{\underline{\mathbf{V}}}^T \hat{\mathbf{u}}(\mathbf{k}, \omega), \quad \text{(A-6)}$$

where $\hat{\underline{\mathbf{Q}}}$ is a diagonal matrix with elements

$$\hat{q}_{ii}(\omega, \Delta t, \mathbf{k}) = \sin^2\left(\frac{\omega \Delta t}{2}\right) + \frac{1}{2} \sum_{n=1}^{N} (-1)^n \frac{\Delta t^{2n}}{(2n)!} \lambda_i^{2n}(\mathbf{k}) \tag{A-7}$$

These equations represent the conditions allowing waves to propagate through the elastic medium. They determine the velocities and the polarizations of the three body-wave types. This system has nontrivial solutions if and only if

$$|\hat{\mathbf{Q}}| = 0, \tag{A-8}$$

which is equivalent to

$$\hat{q}_{11}\hat{q}_{22}\hat{q}_{33} = 0. \tag{A-9}$$

We can express the frequency as a function of the numerical wavenumber and the time increment Δt

$$\tilde{\omega}(\mathbf{k}, \Delta t) = \frac{2}{\Delta t} \arcsin \sqrt{-\frac{1}{2} \sum_{n=1}^{N} (-1)^n \lambda_i^{2n}(\mathbf{k}) \frac{\Delta t^{2n}}{(2n)!}}, \tag{A-10}$$

which is used to calculate the phase velocity $c(\mathbf{k})$

$$c(\mathbf{k}) = \frac{\omega(\mathbf{k})}{|\mathbf{k}|}, \tag{A-11}$$

and the group velocity $g(\mathbf{k})$

$$g_i(\mathbf{k}) = \frac{\partial \omega(\mathbf{k})}{\partial k_i}. \tag{A-12}$$